Gigahertz laser resonant ultrasound spectroscopy for the evaluation of transverse elastic properties of micrometric bers

Denis Mounier, Christophe Poilane, Haithem Khelfa, Pascal Picart

Gigahertz laser resonant ultrasound spectroscopy for the evaluation of transverse elastic properties of micrometric fibers

Denis MOUNIER[b,d,*], Christophe POILÂNE[c], Haithem KHELFA[a], Pascal PICART[a,d]

[a] *LUNAM Université du Maine, Laboratoire d'Acoustique de l'Université du Maine (LAUM), UMR CNRS 6613, Avenue Olivier Messiaen, 72085 Le Mans cedex 9, France*
[b] *LUNAM Université du Maine, Institut des Molécules et des Matériaux du Mans (IMMM), UMR CNRS 6283, Avenue Olivier Messiaen, 72085 Le Mans cedex 9, France*
[c] *Centre de Recherche sur les Ions, les Matériaux et la Photonique, (CIMAP Alençon), UMR6252 ENSICAEN-UCBN-CNRS-CEA, IUT d'Alençon, 61250 Damigny, France*
[d] *Ecole Nationale Supérieure d'Ingénieurs du Mans, rue Aristote, 72085 Le Mans cedex 9, France*

Abstract

The cross section eigenmodes of micrometric cylinders were measured in the range of several tenth of MHz to about 0.5 GHz. The vibrations were excited using subnanosecond laser pulses. The cross section eigenmodes were simulated using finite element modeling in a 2D geometry. Using the method of resonant ultrasound spectroscopy, the vibration spectrum of an aluminum wire of diameter 33 µm served to determine the transverse Young modulus and Poisson ratio with a precision of 0.7% and 0.3%, respectively. The calculated and measured frequencies of cross section eigenmodes were fitted with a precision better than 0.5% in the 50-500 MHz range.

Keywords:
fiber, laser ultrasonics, resonant ultrasound spectroscopy (RUS), finite element modeling, laser interferometry, cylinder, eigenmodes, Rayleigh modes, wave gallery modes, design of experiment (DOE)

1. Introduction

Resonant ultrasound spectroscopy (RUS) has been extensively used during the past two decades to evaluate the elastic constants of various anisotropic solid materials with an ulti-

*Corresponding author
Email address: denis.mounier@univ-lemans.fr (Denis MOUNIER)

mate precision [1–4]. From the measurement of the mechanical resonance frequencies of a sample, the elastic constants of the material can be determined.

The PZT-RUS method, *i.e.* the RUS technique using piezoelectric transducers for both the excitation and the measurement of vibrations, is the most widely used technique. The optimum size of the sample for PZT-RUS is about 1 cm, but the technique can be used for small samples whose dimensions are of the order of 0.5 mm with specially designed transducers [3]. For such small samples, the RUS technique may require the measurement of resonance frequencies up to 50 MHz [5].

However, even in the case of samples of several millimeters in size, contact forces between the ultrasonic transducers and the sample may lead to spurious frequency shifts for the resonance frequencies in addition to the widening of resonances [6–8]. The problem of contacts comes up more and more crucial as the size of samples decreases.

The suppression of contact forces by using lasers for both the excitation and the detection of vibrations results in getting sharp resonances, which is beneficial to the accuracy of measurement [7, 8]. The excitation of vibrations can be carried out by using a periodic laser modulation, whose frequency is swept over the required range [9]. Alternatively, short laser pulses can be used to excite the vibrations of the sample. The advantage of the pulsed method lies in the possibility of exciting simultaneously many eigenmodes over a very large frequency range. The broad band excitation provided by short optical pulses is particularly appropriate to the study of very small samples. The vibrations are measured in the time domain and the eigenfrequencies are obtained from the Fourier transform of the measured signal. The pulsed Laser-RUS method is preferable to determine the elastic constants of small samples [7, 8, 10, 11] or to detect flaws in a small composite structure [12–15]. In this paper, we present a pulsed LRUS technique applied to the evaluation of elastic constants of micrometric fibers, whose diameters are in the range 5-50 µm. For such small dimensions, the eigenfrequencies must be measured in the 0.05-1 GHz range.

The LRUS allows one to evaluate the elastic constants on a single fiber, in contrast with indirect methods of evaluation [16]. From the evaluation of the elastic constants of a unidirectional fiber composite, the elastic constants of the fibers are calculated. This indirect

method is based on specific assumptions about the nature of the reinforcing effect of fibers in the polymer matrix. These assumptions may not be valid for all kinds of reinforced polymers, so the application of this method may lead to erroneous results. Therefore, it is is much more reliable to evaluate the elastic constants directly on a single fiber.

A direct evaluation of elastic constants of carbon fibers by a non-contact technique was first achieved using the technique of laser picosecond ultrasonics [17]. The transverse elastic constant C_{11} of carbon fibers was evaluated through the measurement of the time of flight of acoustic pulses that propagate back and forth across a fiber diameter, which determines the longitudinal acoustic velocity and then the C_{11} elastic constant. However, the evaluation of the C_{44} elastic constant, which requires the measurement of the transverse acoustic velocity, could not be achieved because of the difficulty to generate and to detect picosecond transverse acoustic waves.

Fibers are commonly used in reinforced polymers, such as glass or carbon fibers. The interest of the method is great for anisotropic fibers (carbon and vegetal fibers) because of the lack of reliable and accurate methods for the evaluation of the elastic constants of fibers, in particular the elastic constants characterizing the transverse elastic properties. The evaluation of the longitudinal Young modulus of fibers is generally carried out using the tensile test method [18, 19]. But this method is impracticable to measure the transverse elastic properties.

We illustrate the application of the LRUS method to the evaluation of the transverse Young modulus and Poisson ratio of a micrometric aluminum wire. The evaluation of the transverse elastic properties of fibers requires the excitation of the *cross section* eigenmodes. In our approach, the propagation of guided acoustic waves along the fiber axis is neglected, so the mechanical displacements are restricted to a plane perpendicular to the fiber axis. The restriction in 2D of the cylinder vibrations results in a discrete vibration spectrum, which is required for the application of the RUS method. In section 2, we will describe the experimental method used to excite and detect cross-section modes of a fiber. In section 3, we will present the method used to solve the inverse problem, which leads to the evaluation of the transverse elastic properties of an aluminum fiber. We will also discuss the conditions

of validity RUS applied to a cylinder.

2. Measurement of ultrasonic vibrations

2.1. Laser ultrasonic setup

The irradiation of a cylinder with a laser pulse can excite many acoustic guided modes. The propagation of guided modes along the cylinder axis is determined by the dispersion relation $\omega(k)$, where k is the propagation wave vector along the cylinder axis and $\omega/(2\pi)$ is the frequency of the guided mode. The dispersion relation determines both the phase velocity $v_\phi = \omega/k$ and the group velocity $v_g = d\omega/dk$ of the guided mode.

Both the geometry of the laser spot focused on the cylinder surface and the duration of the laser pulse determine the spectral range of guided modes that can be excited. If the pump beam is focused to form a linear spot parallel to one of the generating line of the cylinder, then a linear acoustic source will be formed and a cylindrical acoustic wave propagating perpendicularly to the cylinder axis will be generated. Consequently, a linear acoustic source parallel to the cylinder axis, which is very long compared to the fiber diameter will favor the excitation of guided modes which very small wave vectors $k \approx 0$, *i.e.* with very large wavelengths $\lambda = 2\pi/k$ compared to the fiber diameter. Moreover, such a linear acoustic source will force the displacements in the directions perpendicular to the cylinder axis and the displacements will be almost independent of the z-coordinate around the center of the acoustic source.

Figure 1 shows the LRUS setup, which includes two parts: the first part is devoted to the excitation of vibrations and the second part, the interferometer, serves to measure ultrasonic vibrations. The vibrations of fibers are excited using a Q-switched Nd:YAG microchip laser at 1064 nm from *TEEM photonics* whose pulses have a maximum energy of 10 µJ and a duration of 0.6 ns at a maximum repetition rate of 5 kHz. With a 0.6 ns pump pulse, it is possible to generate vibrations up to the 1-2 GHz frequency range, which is sufficient to excite many eigenmodes of a fiber whose diameter is in the 5-50 µm range.

The fibers are mounted on a 1 cm diameter plastic ring (Inset of Fig. 1, at the bottom right). In order to excite acoustic waves which propagate mainly perpendicularly to the

Figure 1: Experimental setup of laser ultrasonic resonance spectroscopy (L-RUS) and support of the fiber. BS: beam splitter, PBS : polarizing beam splitter, VA: variable attenuator, $\lambda/4$: quarter-wave plate, $\lambda/2$: half-wave plate, M1, M2, M3, M4: mirrors, PZT: piezoelectric actuator, GD: ground potential.

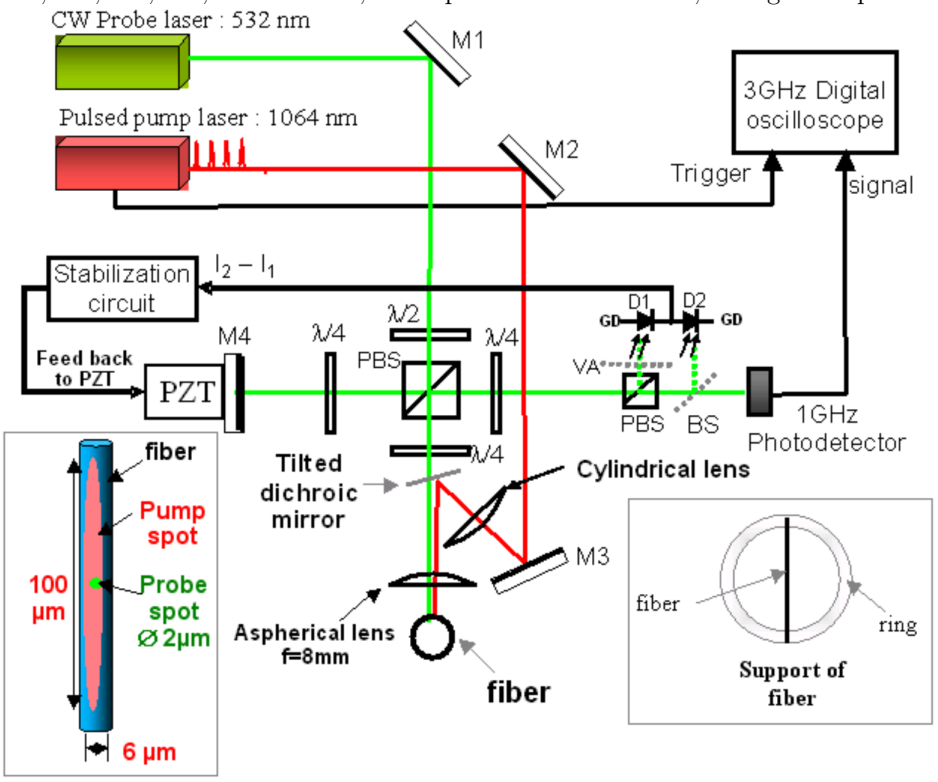

fiber axis, the length of the pump spot must be much larger than the fiber diameter. The pump laser is therefore shaped to form a narrow line, parallel to the fiber axis. By using a cylindrical lens placed in the optical path of the pump beam, we obtain an elliptical spot with dimensions 6 µm × 100 µm at the fiber surface, with the main axis of the ellipse aligned with the fiber axis (see left inset of Fig. 1). By a proper adjustment of the pulse energy with an variable attenuator (not represented on Fig. 1), the vibrations of the fiber can be excited in the non destructive thermoelastic regime [20].

For the measurement of radial ultrasonic vibrations, a stabilized homodyne Michelson interferometer is used [20]. The probe beam at 532 nm is focused onto the fiber surface using an aspherical lens (x20) having 8 mm focal length and 0.5 numerical aperture. The resulting focused spot centered on the pump line has a diameter of about 2 µm (inset of Fig. 1). An incident probe power of 1-2 mW is sufficient to achieve a measurement sensitivity of

$1\,\mathrm{mV\,nm^{-1}}$ on a metallic surface.

The optical interferometric signal is received by a high-speed photodetector with a band-pass of 1 GHz. Using a digital oscilloscope with a band-pass of 3 GHz, the signals are recorded in synchronization with the pump pulses during about 2 µs after the pump laser pulse. Thanks to the averaging of 10 000 acquisitions, which necessitates a only two seconds at the pulse repetition rate of 5 kHz, we obtain a detection threshold of about 5 pm for the measurement of out-of-plane displacements, which is sufficient to detect the vibrations with a satisfactorily signal to noise ratio.

The high frequency ultrasonic vibrations are superimposed to a slow and huge displacement of the fiber; a displacements of about 5-10 nm which is probably induced by the sudden expansion of the air in contact with the heated fiber surface, thus inducing the recoil of the fiber. This slow drift of the signal is filtered out in order to magnify the high frequency vibrations corresponding to the fiber *cross-section eigenmodes*. The vibration spectrum is obtained with 0.5 MHz resolution by calculating the Fast Fourier Transform (FFT) of the digitized signal (Fig. 2).

2.2. Vibration spectrum of an aluminum wire

The test sample is an aluminum bonding wire with 1% silicon, manufactured by *HERAEUS* [21]. With a scanning electron microscope (SEM), we measured the wire diameter at several points of the wire. A mean diameter of (32.7 ± 0.1) µm was determined over a length of 1 cm.

The ultrasonic measurements were made at several points each millimeter over a wire length of 5 mm.

Figure 2 shows one of the measured vibration spectra of the aluminum wire. The inset of Fig. 2 represents the high frequency ultrasonic component used to calculate the vibration spectrum. Each eigenfrequency can be determined with an accuracy of about 0.5 MHz. For each spectral line, the mean frequency and standard deviation were calculated from the vibration spectra measured at different points of the wire. The standard deviations was found of the order of the spectral resolution 0.5 MHz. The repeatability of the vibration

Figure 2: Eigenfrequency spectrum of an aluminum wire of diameter 32.7 µm calculated from the signal shown in the inset, which shows the high frequency component of the recorded signal, corresponding to the vibrations of the wire cross-section.

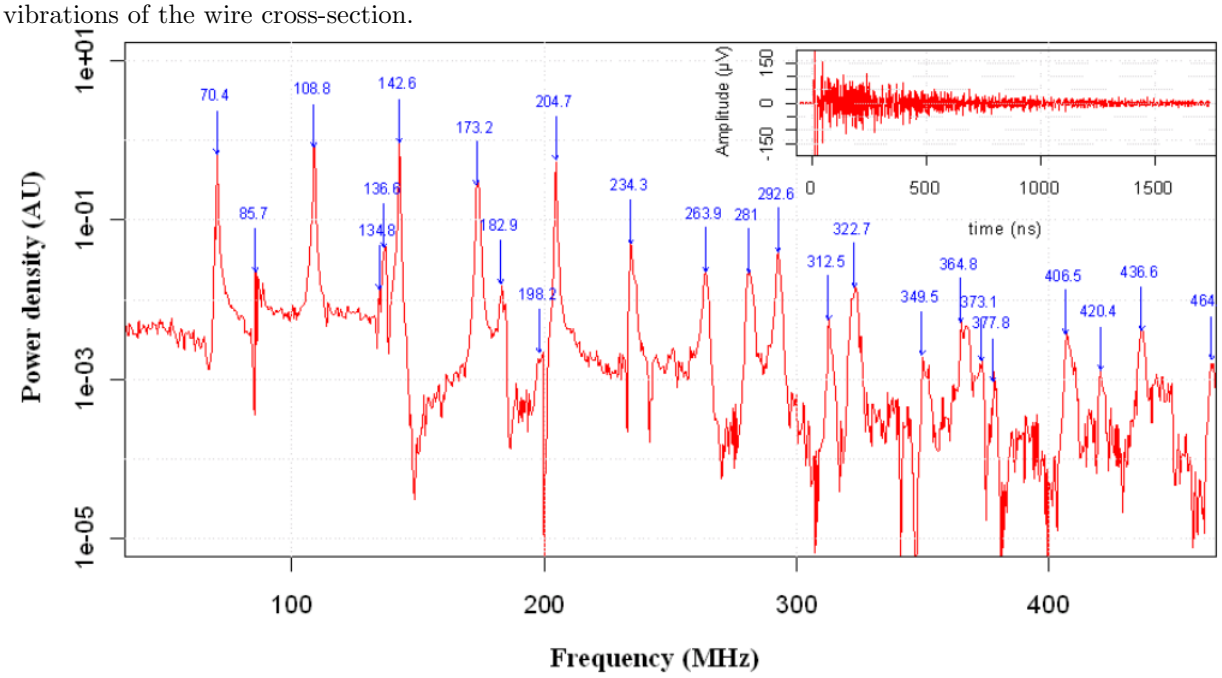

spectra assesses the constancy of the wire diameter over a length of 5 mm.

The next step before determining the transverse Young modulus and Poisson ratio of the aluminum wire is the identification of eigenmodes.

3. Evaluation of the transverse elastic properties of an aluminum fiber

3.1. Two-dimensional finite element modeling

In the following, we will focus our attention on $k = 0$ guided modes, whose displacements are restricted within the xy-plane. From the experimental conditions depicted before, we expect that the excited eigenmodes are mainly the $k = 0$ guided modes. We will refer to such guided modes as *cross-section* modes. The eigenfrequencies of cross-section modes depend only on the transverse Young modulus and Poisson ratio of the cylinder. Consequently, from the measured eigenfrequencies, the transverse Young modulus and Poisson ratio can be determined.

A 2D mechanical model of the aluminum wire is carried out. It is assumed that the elastic properties are homogeneous and invariant by rotation around the fiber axis, *i.e.* the mechanical properties of the material are *transverse isotropic*. Thus, the eigenmodes are determined by: the cylinder diameter d, the Young modulus E, the Poisson ratio ν and density ρ. The vibration eigenmodes of an aluminum wire are determined with the software *COMSOL Multiphysics*. The mode shapes of the first 20 eigenmodes are illustrated in Fig. 3.

3.1.1. Nomenclature of modes

The guided modes of a cylinder are named according to the nomenclature of Silk and Bainton [22]. The modes are labeled $X(m,n)$ (or simply Xm,n as in Fig. 4 or Table 1) where $X = L, T,$ or F and m, n are positive integers. The letters L, T or F are the initials of *longitudinal*, *torsional* and *flexural* modes, respectively. The number m of a $X(m,n)$ mode characterizes the rotational symmetry of the mode shape and n the ordering of the Xm mode in the frequency scale. In cylindrical coordinates (r,θ,z), the u_r and u_θ components of the displacement field vary according to the functions $\cos m\theta$ or $\sin m\theta$, which means that the mode shape is invariant after a rotation of $2\pi/m$ rad around the cylinder z-axis. The longitudinal and torsional modes, which have both a rotational symmetry for an arbitrary rotation angle around the cylinder axis have $m = 0$. The *longitudinal* and the *torsional* modes are characterized by the displacements $u_\theta = 0$ and $u_r = 0$, respectively. The modes with $m > 0$ are *flexural modes*.

According to Victorov [23, 24], the cross-section modes belong to one of the two categories: the *Rayleigh modes* (R) or the *Wave Gallery modes* (WG). The *Rayleigh modes* are flexural modes of the $n = 0$ series, which we denote more explicitly $R(m,0)$ instead of $F(m,0)$. The Rayleigh modes series starts with the $R(2,0)$ mode, as the $R(1,0)$ mode is the trivial Rayleigh mode corresponding to the translation of the cylinder along a radial direction, having thus the frequency zero. The *WG modes* are denoted $WG(m,n)$ instead of $F(m,n)$, with $n > 0$ and $m > 0$. The first *longitudinal mode*, denoted $L(0,1)$, is often called the *breathing mode*. The first *torsional mode* is denoted $T(0,1)$. The $L(0,0)$ and $T(0,0)$

modes are trivial modes with their eigenfrequency equal to zero.

The distinction between *Rayleigh* and some series of *Wave Gallery* modes will be useful to consider in the perspective of mode identification, as all Rayleigh modes have significant radial components u_r and weak orthoradial components u_θ at the surface of the cylinder. On the contrary, the $n = 1$ series of Wave Gallery modes is characterized by weak radial components compared to the orthoradial ones and the displacements are mainly concentrated in the vicinity of the surface. The displacements for WG modes of the series $n > 1$ may have very weak components at the surface. In contrast, for some particular WG modes (for example see mode 12 in Fig. 3 and Table 1), the magnitude of the radial displacement may be significant. Considering the correlation between the relative magnitude of radial displacements predicted by the modeling and the amplitudes of the spectral lines may help to identify the modes (cf. section 3.2).

The longitudinal modes $L(0, n)$ and the torsional modes $T(0, n)$ are not degenerate. On the contrary, the $m > 0$ modes are two-fold degenerate. This property arises from the existence of the two angular functions $\cos m\theta$ and $\sin m\theta$, expressing the angular dependence of a mode shape. The two degenerate mode shapes can be deduced from each other by a rotation of $\pi/(2\,m)$ rad. If a fiber deviates a little from the circular symmetry, a degeneracy lifting may occur. If the spectral resolution is sufficient, it could be possible to appreciate an elliptical shape of the fiber cross-section. In the spectrum of Fig. 2, the absence of doublets in the spectrum demonstrates the almost perfect circular cross-section of the aluminum wire.

3.2. Modes identification

The RUS technique requires the correct mode identification of each measured eigenfrequency. This can be done by determining experimentally the mode shapes, which can be then compared to the calculated ones [10, 25]. A raster-scanning of the probe laser on the surface can image the mode shape.

However, in the case of a non-planar surface, like a fiber, it is not possible to scan the probe laser and thus to determine experimentally the mode shapes. Nevertheless, the digital holography technique could be an alternative to determine experimentally the mode

shapes of fibers [26, 27], but this technique is not yet implemented for small object as fibers. therefore, we will try to guess which eigenmode corresponds to each measured eigenfrequency.

The Rayleigh eigenmodes are characterized by strong radial components at the surface and would thus be more likely attributed to the strongest lines of the spectrum. Indeed, Raleigh modes can be observed in the spectrum up to the order $m = 15$ (eigenfrequency at 464 MHz). Conversely, WG modes which have predominant orthoradial components at the surface would correspond to spectral lines of smaller amplitude. The torsional modes, with zero radial components, are missing modes.

Eigenfrequencies up to about 200 MHz are well separated in the spectrum and can be identified without ambiguity, except for the two close lines at 135 MHz and 137 MHz, which may be attributed either to the first longitudinal mode $L(0,1)$ (the breathing mode) or to the $WG(2,1)$ mode. The strongest line at 137 MHz would correspond more likely to the $L(0,1)$ mode (mode 5), as this mode has exclusively radial components. The $WG(2,1)$ mode (mode 4 in Fig. 3) displays very weak radial components, so it would thus more likely corresponds to the weakest spectral line.

The mode identification can be carried out without ambiguity for 9 eigenfrequencies among the first 11 eigenfrequencies shown in Table 1. The values in Table 1 corresponds to the mean experimental frequencies measured on several spectra. Most of the frequencies displayed in Fig. 2 are close to the frequencies of Table 1 within 0.5 MHz.

3.3. Solving the inverse problem

In order to determine the mechanical parameters, we have to search the set of mechanical parameters which minimizes the root mean square of the distance between the experimental frequencies f_i^{exp} and the calculated ones f_i^{calc}, which is:

$$\sigma_{res} = \sqrt{(1/N)\sum_{i=1}^{N}(f_i^{exp} - f_i^{calc})^2} \qquad (1)$$

A non linear regression algorithm (Gauss-Newton) where N is the number of the experimental frequencies that are considered for the fit. Only frequencies below 210 MHz are

considered, as these lines can be identified without ambiguity. Eigenfrequencies beyond 210 MHz have been omitted, as the overlap of some unresolved spectral lines may lead to an ambiguous identification. Only 9 eigenfrequencies among the 11 below 210 MHz can be identified unambiguously. We do not consider the weak line around 135 MHz, probably the $WG(2,1)$ mode, which is visible only a few times among all the measured spectra, and thus this line cannot be measured accurately. The torsional $T(0,1)$ mode, which is missing in the spectra, is not considered.

Solving an inverse problem requires in general many iterations. For each iteration, the eigenfrequencies are calculated for a set of input parameters. The use of finite element calculation is not very practicable for iterative processes. For a cylindrical fiber, an analytic calculation of eigenfrequencies would be probably the best method to calculate the eigenfrequencies. However, we preferred to use a more general method which can be applied to a fiber of arbitrary cross-section shape. In order to calculate quickly the eigenfrequencies for a given set of the parameters E, ν and ρ, we determined first the coefficients of polynomial interpolation functions, which can be used to calculate the eigenfrequencies. For a predetermined diameter d_0, each interpolation function can be expressed in the form of a Taylor series of the three variables E, ν and ρ, which can be express in the form:

$$f_i(E,\nu,\rho) = \sum_{\alpha,\beta,\gamma} C_i^{\alpha\,\beta\,\gamma} (E-E_0)^\alpha \, (\nu-\nu_0)^\beta \, (\rho-\rho_0)^\gamma \tag{2}$$

where $E_0 = 70\,\mathrm{GPa}$ and $\nu_0 = 0.33$ and $\rho_0 = 2700\,\mathrm{kg/m^3}$.

A second-order Taylor series is sufficient to get an accurate prediction of the frequencies, so that only 10 coefficients are determined, those verifying the inequality $\alpha+\beta+\gamma \leq 2$. For each frequency i, the 10 coefficients $C_i^{\alpha\,\beta\,\gamma}$ were determined from a set of 15 finite element models with the parameters (E,ν,ρ) suitably chosen inside the 3-dimensional domain $\mathbf{D}$ defined by the intervals: $E = (70 \pm 3)\,\mathrm{GPa}$, $\nu = 0.33 \pm 0.03$ and $\rho = (2700 \pm 75)\,\mathrm{kg/m^3}$. The method of *design of experiment* (DOE) for quadratic models [28] was used for this purpose.

The interpolation functions of Eq. 2 are used to predict the eigenfrequencies with an

error inferior to 0.05 MHz in the **D**-domain, which is sufficient compared to the experimental uncertainties.

For a different diameter d of the cylinder, the eigenfrequencies were calculated by first using Eq. 2 and by multiplying the eigenfrequencies vector by the scale factor d_0/d.

3.4. Results

With the 9 interpolation functions, we searched the set of parameters (E, ν, ρ) which minimizes the standard residual σ_{res}. For the first run, we fixed the diameter, the Young modulus and the density: 32.7 µm, 70.0 GPa and 2700 kg/m^3. We found that the best fit is obtained with $\sigma_{res} = 0.47$ MHz when the Poisson ratio $\nu = 0.3496$. If the diameter and the density are fixed to the preceding values, the best fit is $E = 69.6$ GPa and $\nu = 0.350$, which is obtained with $\sigma_{res} = 0.17$ MHz. No significant improvement of the fit can be obtained by varying the density.

Table 1: Measured and calculated eigenfrequencies in MHz, corresponding to the mode shapes of Figure 3. The right column shows the differences: $\Delta f = f_{exp} - f_{calc}$.

	mode	f_{exp}	f_{calc}	Δf		mode	f_{exp}	f_{calc}	Δf
1	R2,0	70.54	70.67	-0.13	11	R6,0	204.71	204.44	0.27
2	WG1,1	86.15	86.54	-0.39	12	WG1,3	233.02	233.37	-0.35
3	R3,0	109.07	108.99	0.08	13	WG4,1	234.28	233.55	0.73
4	WG2,1	134.72	135.10	-0.38	14	R7,0	235.11	234.33	0.79
5	L0,1	136.97	136.92	0.06	15	WG2,2	241.98	240.70	1.28
6	R4,0	142.47	142.49	-0.01	16	T0,2	NA	253.17	NA
7	T0,1	NA	154.47	NA	17	R8,0	264.02	263.83	0.19
8	R5,0	173.87	173.97	-0.10	18	WG5,1	280.83	280.62	0.22
9	WG3,1	184.64	184.69	-0.05	19	WG3,2	281.62	282.05	-0.43
10	WG1,2	198.33	198.27	0.05	20	R9,0	292.70	293.09	-0.39

In order to evaluate the measurement uncertainty for the Young modulus and the Poisson ratio, due to the measurement uncertainty of the fiber diameter, we supposed that the fiber

diameter is now 32.8 µm. The best evaluation of the parameters is $E = 70.0\,\mathrm{GPa}$ and $\nu = 0.350$ with $\sigma_{res} = 0.17\,\mathrm{MHz}$. Therefore, an error in the evaluation of the fiber diameter of 0.1 µm propagates an error of 0.4 GPa in the Young modulus. But it is remarkable that the Poisson ratio is not sensitive to the diameter uncertainty. The evaluation of the Young modulus is also sensitive to the density, with a sensitivity $\partial E/\partial\rho = 0.026\,\mathrm{GPa}/(\mathrm{kg/m^3})$. If the uncertainty of the fiber density is neglected, the result is $E = (69.6 \pm 0.4)\,\mathrm{GPa}$ and $\nu = 0.350 \pm 0.001$.

The Young modulus and the Poisson ratio were determined by considering only 9 experimental frequencies below 210 MHz. We must verify now if determined parameters give the correct prediction of the other eigenfrequencies. Table 1 shows the comparison between the experimental and calculated frequencies up to 300 MHz with the parameters $d = 32.7\,\mu\mathrm{m}$, $E = 69.6\,\mathrm{GPa}$, $\nu = 0.350$ and $\rho = 2700\,\mathrm{kg/m^3}$. Each experimental frequency f_{exp} is an average of several measured eigenfrequencies. The relative errors $\Delta = (f_{exp} - f_{calc})/f_{calc}$ remain under 0.5% for all the calculated frequencies below 300 MHz. The $WG(2,1)$ mode is located before the "breathing" $L(0,1)$ mode, in agreement with our initial guess.

Moreover, the correlation between the calculated and the experimental frequencies is quite good for 31 modes up to the frequency of the Rayleigh mode $R(15,0)$, which is calculated at 466 MHz and measured at 464 MHz. The relative residuals $\Delta = (f_{exp} - f_{calc})/f_{calc}$ are plotted in Fig. 4. For all the measured eigenfrequencies the relative error is below 0.5%.

3.5. The limits of the 2-dimensional approach

Though the 2D model is capable to fit rather well most of the measured eigenfrequencies, it cannot explain some particular features observed in the experimental spectrum, in particular the unexpected weakness of the "breathing mode" line at 137 MHz.

In the 2D approach, the propagation of acoustic waves along the fiber axis is neglected. We implicitly assume that the group velocities of the excited guided modes are zero. In order to evaluate an upper limit for the group velocity, we must take into account of the finite length of the pump line, which determines a cutoff in the wave vector spectrum of the excited guided modes. The cutoff wave number is roughly $1/L_p = 1/0.1 = 10\,\mathrm{mm^{-1}}$,

where L_p is the length of the pump spot. The propagation of guided modes can be ignored during the acquisition time $T_a = 2\,\mu s$ only if their group velocity is much lower than $v_g^{max} = L_p/T_a = 50\,\mathrm{m\,s^{-1}}$. In consequence, the 2D approach is valid only if the group velocity is inferior to $50\,\mathrm{m\,s^{-1}}$ for all wave vectors $k \lesssim 2\pi \cdot 10\,\mathrm{mm^{-1}}$.

The group velocity is zero for pure cross-section modes, *i.e.* with the $k = 0$ guided modes. But for some modes, the variation of the group velocity with k may be too rapid between the zero and the cutoff wave vector $k_{max} = 2\pi \cdot 10\,\mathrm{mm^{-1}}$ and this would result in a quick vanishing signal and thus a strong apparent damping of the measured vibrations. In the spectral domain, this will result in weak and broad spectral line.

The fact that most of the spectral lines displayed in Fig. 2 have relatively high amplitudes proves *a posteriori* that the group velocities of most guided modes are not much larger than the above estimated value $50\,\mathrm{m\,s^{-1}}$. However, the condition $v_g < 50\,\mathrm{m\,s^{-1}}$ may not be fulfilled for some modes, in particular for the breathing mode.

The 2D model does not take into account the possible Zero Group Velocity modes (ZGV) that may be excited in a cylinder. Such modes are known in structures capable of guiding acoustic waves, such as plates [29]. The existence of ZGV modes in a cylinder is predicted theoretically [30]. The ZGV modes can exhibit very high quality factors in the range of $Q = 1000 - 10000$. Moreover, it is known that ZGV eigenfrequencies are different from the cross-section eigenfrequencies. The differences between cross-section and ZGV eigenfrequencies could explain some discrepancies between the experimental and the calculated eigenfrequencies in the 2D modeling.

4. Conclusion

This paper presents a method to evaluate the transverse Young modulus and Poisson ratio of a micrometric metallic wire by using laser resonant ultrasound spectroscopy. A precision of 0.7% for the Young modulus and 0.3% for the Poisson ratio of an aluminum fiber was achieved.

The pump laser was shaped as a line spot parallel to the fiber axis in order to excite cross section eigenmodes. Using a stabilized homodyne Michelson interferometer, the cross

section eigenfrequencies were measured up to 500 MHz. The 2D vibration model of the wire proved to be in good agreement for about 30 measured eigenfrequencies within an accuracy of 0.5% in the 50-500 MHz range.

Nevertheless, the spectral resolution can be improved by increasing the acquisition time windows, as some modes are not completely damped 2 µs after the excitation. The improved resolution could be useful to detect minute geometrical defects of the cylinder through the observation of the degeneracy lifting of some modes. Furthermore, the measurement of high frequency Rayleigh modes could be useful to probe the mechanical properties of the material in the vicinity of the surface, as the displacements of high frequency Rayleigh modes are localized mainly near the surface.

In order to achieve ultimate precision for the evaluation of the elastic parameters of fibers, it is essential to take into account the propagation of guided modes along the fiber and therefore to carry out the 3-dimensional modeling of the mechanical system and then to determine the eigenfrequencies of the Zero Group Velocity modes (ZGV). Such modes could be useful to improve the precision in the determination of the elastic parameters and could give access to the determination of the intrinsic damping of the material, *i.e.* the imaginary part of the Young modulus.

The application of the LRUS method is not restricted to metallic fibers. We intend to apply more extensively our LRUS method to characterize fibers used in reinforced composite materials, such as carbon, glass, kevlar and vegetal fibers. The study of vegetal fibers, in particular flax fiber, which is a hollow structure approximately cylindrical, requires the association of LRUS with a method to determine the actual geometry of the fiber, such as digital holographic tomography.

References

[1] R. G. Leisure, F. A. Willis, Journal of Physics: Condensed Matter 9 (1997) 6001.

[2] W. M. Visscher, A. Migliori, T. M. Bell, R. A. Reinert 90 (1991) 2154–2162.

[3] A. Migliori, J. D. Maynard, Review of Scientific Instruments 76 (2005) 121301.

[4] B. J. Zadler, J. H. L. Le Rousseau, J. A. Scales, M. L. Smith, Geophysical Journal International 156 (2004) 154–169.

[5] A. Yoneda, Y. Aizawa, M. M. Rahman, S. Sakai, Japanese Journal of Applied Physics 46 (2007) 7898–7903.

[6] A. Yaoita, T. Adachi, A. Yamaji, NDT&E International 38 (2005) 554–560.

[7] P. Sedlák, M. Landa, H. Seiner, L. Bicanová, L. Heller, in: 1st International Symposium on Laser Ultrasonics: Science, Technology and Applications, July-16-18, Montréal, Canada.

[8] S.-K. Park, S.-H. Baik, H.-K. Cha, S. J. Reese, D. H. Hurley, J. Korean Phys. Soc. 57 (2010) 375–379.

[9] S. Sato, K. Inagaki, V. E. Gusev, O. B. Wright, AIP Conference Proceedings 463 (1999) 424–426.

[10] D. H. Hurley, S. J. Reese, F. Farzbod, Journal of Applied Physics 111 (2012) 053527.

[11] N. Nakamura, H. Ogi, M. Hirao, Acta Materialia 52 (2004) 765 – 771.

[12] A. Amziane, M. Amari, D. Mounier, J.-M. Breteau, N. Joly, J. Banchet, D. Tisseur, V. Gusev, Ultrasonics 52 (2012) 39–46.

[13] A. Amziane, M. Amari, D. Mounier, J.-M. Breteau, N. Joly, M. Edely, M. Larcher, P. Noiré, J. Banchet, D. Tisseur, V. Gusev, Proc. of SPIE 8082 (2011) 808224.1–808224.10.

[14] S. Petit, M. Duquennoy, M. Ouaftouh, F. Deneuville, M. Ourak, S. Desvaux, Ultrasonics 43 (2005) 802–810.

[15] F. Deneuville, M. Duquennoy, M. Ouaftouh, M. Ourak, F. Jenot, S. Desvaux, Ultrasonics 49 (2009) 89–93.

[16] R. E. Smith, J. Appl. Phys. 43 (1972) 2555–2561.

[17] D. Ségur, Y. Guillet, B. Audoin, Journal of Physics: Conference Series 278 (2011) 012020.

[18] C. Baley, Composites Part A: Applied Science and Manufacturing 33 (2002) 939 – 948.

[19] C. Sauder, J. Lamon, R. Pailler, Carbon 42 (2004) 715–725.

[20] C. B. Scruby, L. E. Drain, Laser ultrasonics: techniques and applications, 1990.

[21] Heraeus, 2012. AlSi 1%, The Aluminum Fine Wire Solution.

[22] M. Silk, K. Bainton, Ultrasonics 17 (1979) 11 – 19.

[23] I. Viktorov, Rayleigh and Lamb waves, 1967.

[24] D. Clorennec, D. Royer, H. Walaszek, Ultrasonics 40 (2002) 783?789.

[25] H. Ogi, K. Sato, T. Asada, M. Hirao, J. Acoust. Soc. Am. 112 (2002) 2553–2557.

[26] P. Picart, J. Leval, D. Mounier, S. Gougeon, Appl. Opt. 44 (2005) 337–343.

[27] J. Leval, P. Picart, J. P. Boileau, J. C. Pascal, Appl. Opt. 44 (2005) 5763–5772.

[28] Nist/sematech e-handbook of statistical methods, 2012. Response surface designs.

[29] C. Prada, D. Clorennec, D. Royer, The Journal of the Acoustical Society of America 124 (2008) 203–212.

[30] C. Prada-Julia, 2012. Institut Langevin, ESPCI, Paris, confirmed theoretically the existence of ZGV

modes in cylinders (personal communication).

Figure 3: Mode shapes of the first 20 calculated eigenmodes of an aluminum cylinder. Numbers correspond to the ordering numbers of Table 1. Category of each eigenmode: Rayleigh (R), Wave Gallery (WG), longitudinal (L) or torsional (T) is indicated. Rayleigh modes are characterized by predominant radial components. Colors represent the magnitude of the displacements: the deep blue color means a zero displacement, *i.e.* the nodal areas of the mode shape and the red color is for the maximum magnitude. The arrows indicate both the direction and the magnitude of displacements.

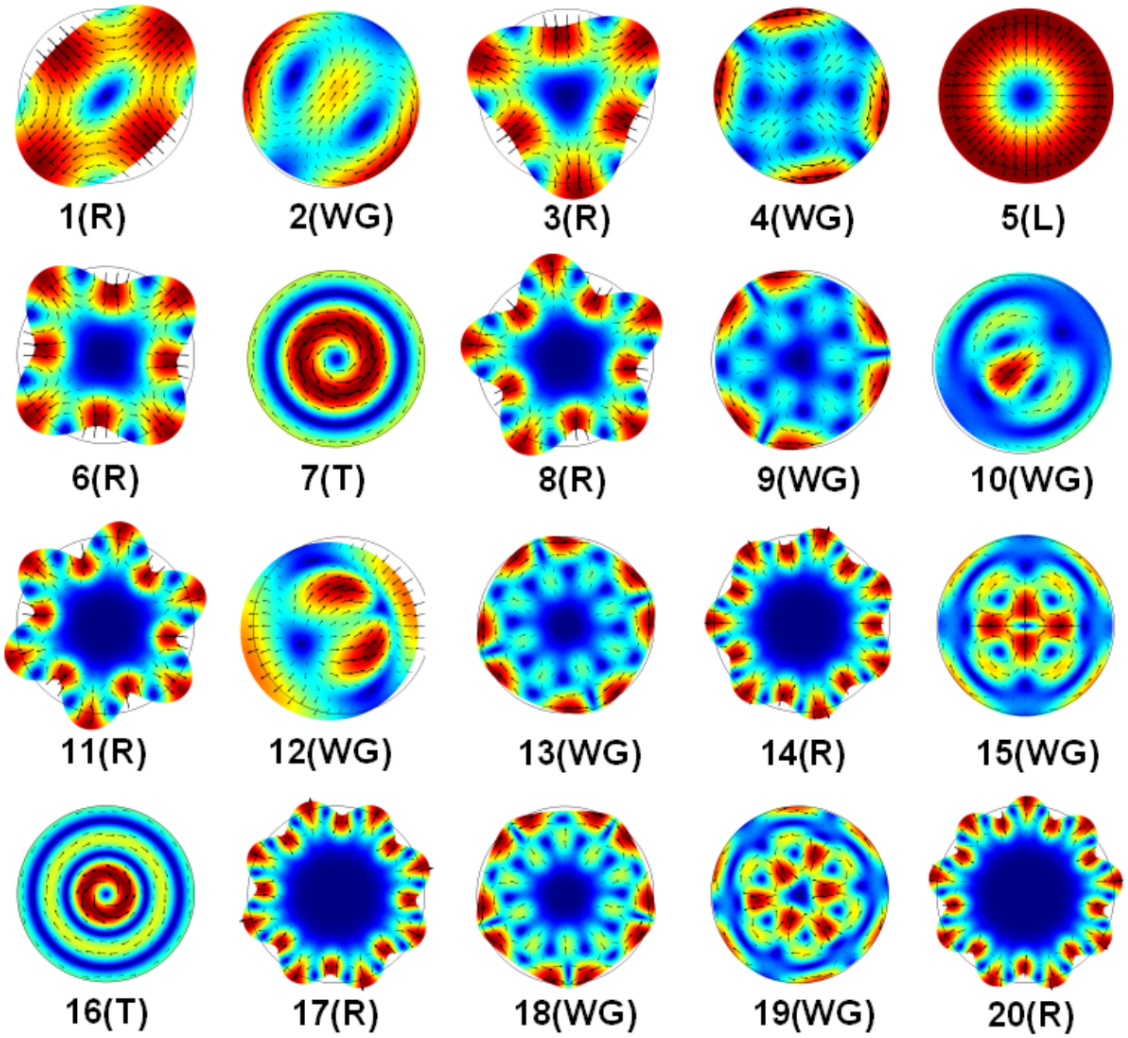

Figure 4: Percentage of relative error between experimental and calculated eigenfrequencies with the parameters: $d = 32.7\,\mu\text{m}$, $E = 69.6\,\text{GPa}$, $\nu = 0.350$ and $\rho = 2700\,\text{kg/m}^3$.